Technical University of Munich
School of Computation, Information and Technology
Chair of Electronic Design Automation

A Power-Aware and Scalable Multi-Topology Design Method for Large-Scale Wavelength-Routed Optical Networks-on-Chip

Bachelor's Thesis

Zijie Ji

Technical University of Munich
School of Computation, Information and Technology
Chair of Electronic Design Automation

A Power-Aware and Scalable Multi-Topology Design Method for Large-Scale Wavelength-Routed Optical Networks-on-Chip

Bachelor's Thesis

Zijie Ji

Supervisor :	M.Sc. Zhidan Zheng
Supervising Professor :	Prof. Dr.-Ing. Ulf Schlichtmann
Topic issued :	11.03.2024
Date of submission :	29.07.2024

Zijie Ji
Felsennelkenanger 11
80937 München

Abstract

Wavelength-routed optical networks-on-chip (WRONoCs) are known for providing high bandwidth, low latency, and low power communication, making them suitable for the growing demands of modern computing and communication environments. It switches signals through microring resonators (MRRs) coupled to different wavelengths, thereby preventing data collisions between optical signals. In WRONoCs, each transmitter and receiver pair has a dedicated data transmission path to ensure collision-free communication simultaneously without arbitration. Various topologies have been proposed to efficiently connect optical signals in WRONoCs. However, as communication demands in WRONoCs continuously grow and the number of cores in multi-core systems increases, the size of a topology becomes larger, which results in a significant increase in the numbers of MRRs, leading to higher maximum insertion loss and an increase in the used number of wavelengths.

In this work, I propose to divide the communication graph of a network into several sub-graphs and use multiple small-scale topologies to support the communications within a sub-graph or among all sub-graphs. To this end, I propose a power-aware and scalable multi-topology design method. To evaluate the performance of my method, I first compared it to a conventional approach, which applies a large topology for the network. The experimental results show that for a 26-core application, my method can reduce wavelength usage and the maximum insertion loss by 54.16% and 52.63%, respectively, compared to the conventional approach. Moreover, I have implemented and compared two typical partitioning methods to my method. My method outperforms the two typical partitioning methods in power efficiency and scalability by reducing the wavelength usage and maximum insertion loss.

Acknowledgments

I would like to express my sincere gratitude to my supervisor, Prof. Dr.-Ing. Ulf Schlichtmann and M.Sc. Zhidan Zheng from the Technical University of Munich, for their responsible guidance and encouragement while writing this thesis.

I am especially grateful to my supervisor, M.Sc. Zhidan Zheng: Her meticulous guidance and patient explanations helped me to complete all the work smoothly. Her dedication to guidance time, early responses, and feedback to my questions greatly encouraged and provided my motivation and confidence. Furthermore, I am deeply thankful for the research opportunity she provided me and her trust in me, which allowed me to learn a lot of state-of-the-art academic ideas that are difficult to encounter during regular studies. Her organizational skills and personal abilities have inspired me to learn from her, motivating me to advance further.

Finally, I would like to thank my family for their support. During the period when I focused on writing my thesis, they provided me with immense emotional support and care. Their considerable concern and understanding gave me substantial motivation for my studies, enabling me to fully dedicate myself to my academic life. Additionally, I would like to thank Taylor Swift for her enchanting music, which added great vitality to my life during the thesis writing process. Having such an outstanding woman as a role model has inspired me to improve myself further.

Contents

List of Figures

List of Tables

1. Introduction

With the rapid advancement of silicon photonics technology, optical networks-on-chip (ONoCs) have emerged to meet the increasing communication demand of multi-core systems. ONoC converts electrical signals into optical signals of different wavelengths and transmits them from a transmitter to a receiver through optical waveguides. ONoC consumes much less power and offers significantly wider bandwidth than current electronic interconnects (P. Grani 2017) (M. Briere 2007).

Wavelength-routed ONoCs (WRONoCs), a specific type of ONoCs, support on-chip communication based on different wavelengths. WRONoCs select and route optical signals with different wavelengths by microring resonators (MRRs). When an optical input signal traverses an MRR, if the wavelength of the input signal matches the resonant wavelength of the MRR, the input signal will be coupled to the MRR and change the transmission direction; otherwise, the input signal will maintain the original direction through the MRR (C. Manolatou 2002). Signal communication in WRONoCs is contention-free and requires no arbitration. Each core on WRONoCs can be either a transmitter or a receiver, and the paths between them are unique, enabling simultaneous communication between transmitters and receivers using different wavelengths (T. Tseng 2019).

Different topologies have been developed to reduce resource waste by reusing MRRs efficiently in WRONoCs, such as GWOR (X. Tan 2011). GWOR can be scaled to support various network sizes and has full communication capability. The connection of GWOR can efficiently reuse MRRs, which reduces the usage of MRRs. Its low power consumption and low latency benefit it for applying on WRONoCs.

However, as the communication demands on WRONoCs increase, the number of required cores in multi-core systems also grows. If the entire WRONoC continues to be supported with a single topology, the size of the required topology will become increasingly significant. As the topology expands, on the one hand, the usage of MRRs will rise, leading to higher insertion loss (L. Duong 2014). On the other hand, the usage of wavelengths will also surge, significantly increasing the power required by the laser source to drive the entire network (M. Ortín-Obón 2017).

To reduce the insertion loss in the topology and the total usage of wavelengths, an approach proposed in this work is to divide large-scale core graphs, i.e., a communication network with many cores, of WRONoCs into multiple small-scale clusters and support every intra-/inter-cluster with small-scale topologies. From one perspective, the wavelength assignment of the intra-clusters is mutually independent, which implies that wavelengths in intra-clusters can be reused, significantly reducing the overall usage of wavelengths. From the other perspective, as

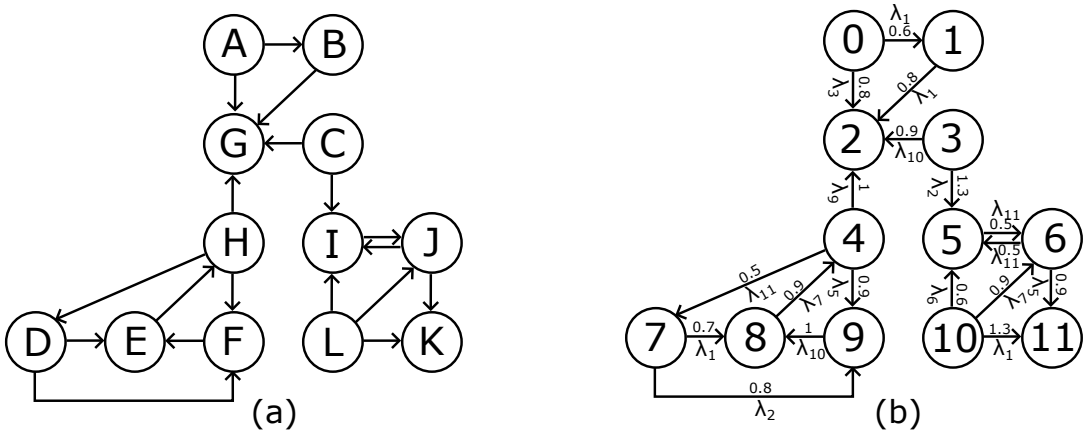

Figure 1.1.: (a) VOPD core graph, (b) Insertion loss and wavelength assignment with a single GWOR topology. The number on each node is the relative input and output ports of the single GWOR. Arrows between two nodes indicate signal communication between the relative cores. The number and λ_x on each edge are the insertion loss and the wavelength assignment of each signal path. x is an integer representing the index of wavelength.

the size of the topology decreases, the number of MRRs that the input signal passes through from the transmitter to the receiver also decreases, leading to lower insertion loss.

A scalable multi-topology design clustering-based method is proposed in this work to divide the core graphs of WRONoCs. After clustering the network with my method, the following example compares supporting an entire network with a single topology and supporting each cluster separately with small-scale topologies. The Video Object Plane Decoder(VOPD) is an application of video processing (D. Bertozzi 2005), and its core graph in Figure 1.1(a) is mapped onto 12 cores. Nodes of the core graph connect with the input and output pairs in a single 12×12 GWOR. Figure 1.1(b) shows each signal path's insertion loss and wavelength assignment of the VOPD core graph connected with a single GWOR. For example, node A is paired with port 0, which represents the input and output pairs of the 12×12 GWOR, and node B is paired with port 1; the insertion loss of signal path from port 0 to port 1 is 0.6 dB; the assigned wavelength is λ_1. Figure 1.2 shows each signal path's insertion loss and wavelength assignment of inter- and intra-clusters in the VOPD core graph clustered by my method. The comparison of the maximum insertion loss and wavelength usage with a single GWOR topology and with multiple GWOR topologies is shown in Tablet 1.1. The experimental results show that the maximum insertion loss for the VOPD core graph is reduced by 0.7 dB, and wavelength usage is reduced by 5. Dividing the network into multiple clusters and supporting with multiple small-scale topologies can improve the network's insertion loss and wavelength usage and reduce the power consumption.

To evaluate the performance of my clustering method, I applied it to multiple core graphs and compared the results to the conventional approach, which applies a large topology for the network. Furthermore, I have implemented and compared two typical partitioning methods to my method. The results demonstrate that using my method significantly improves the

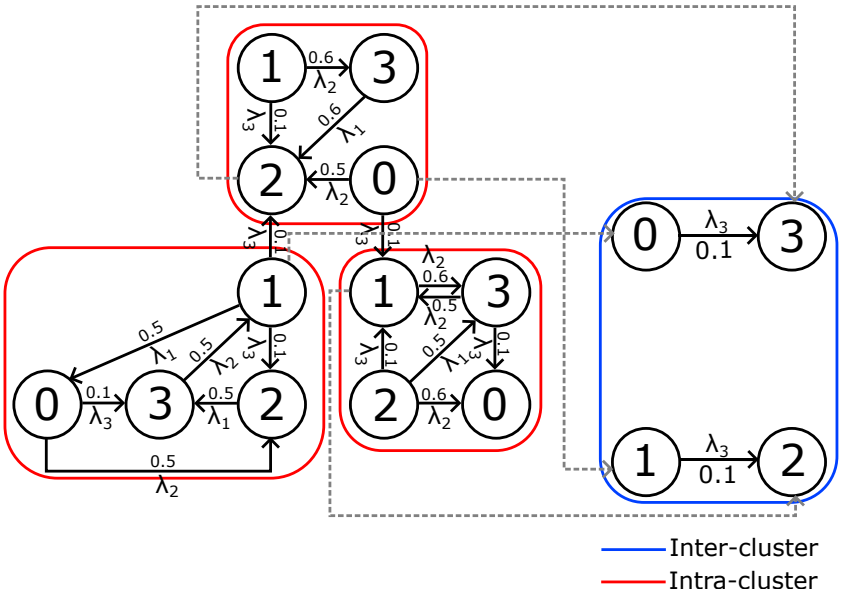

Figure 1.2.: Insertion loss and wavelength assignment with multiple GWOR topologies.

	Maximum Insertion Loss	Wavelength Usage
A single GWOR topology	1.3 dB	9
Multiple GWOR topologies	0.6 dB	4

Table 1.1.: Comparison of maximum insertion loss and wavelength usage.

network's maximum insertion loss and wavelength usage. For example, the wavelength usage and maximum insertion loss of a 12-core application, Video Object Plane Decoder (VOPD), reduce respectively 55.55% and 57.14%. Additionally, I implemented two typical partitioning algorithms: the Kernighan-Lin algorithm and the Stoer-Wagner minimum cut algorithm and compared them to my method. Besides, I proposed two node-pairing methods for pairing the nodes of core graphs and the input and output pairs of topologies. Both node-pairing approaches can effectively reduce the maximum insertion loss in the clustered network.

2. Background

2.1. Introduction of a typical WRONoC environmental setting

One of the most widespread environmental settings of WRONoCs consists of an electronic layer and an optical layer stacked perpendicularly to each other. The electronic layer typically houses most electronic circuits, while the optical layer accommodates MRR, digital circuits, photodetectors, and other components. An array of off-chip continuous wave laser sources drives the optical layer, which uses different wavelengths to route throughout the entire optical layer (M. Ortín-Obón 2017) (Z. Zheng 2021b).

2.2. Optical switching elements

Optical switching elements are formed by waveguides and MRRs. An MRR is an optical component. When the wavelength of a signal matches the resonant wavelength of the MRR, the signal is coupled to the MRR and switched to the corresponding waveguide. Otherwise, the signal keeps its original path. The radius of the MRR determines its resonant wavelength (C. Manolatou 2002).

MRR features two coupling mechanisms: the parallel switching element (PSE) and the crossing switch element (CSE). PSE places an MRR between a pair of parallel waveguides, which accepts the rotated 180° waveguide direction, as shown in Figure 2.1. CSE positions an MRR at a pair of crossing waveguides. It can accept both the clockwise rotated 90° or 270° waveguide direction. Figure 2.4 shows the schematic diagram of two CSE working mechanisms. According to the structure of topologies, most topologies prefer the CSE with 90° signal path because 270° signal path produces more insertion loss (Z. Zheng 2021a). The coupling mechanisms give rise to various topological structures.

2.3. Introduction of GWOR

Most topologies widely researched are based on the CSE 90° drop coupling mechanism, such as GWOR (X. Tan 2011). GWOR is scalable to support diverse network sizes and supports full communication, meaning any core can communicate with others except itself. The connection of GWOR can reuse MRRs efficiently, which reduces the usage of MRRs. Meanwhile, its low

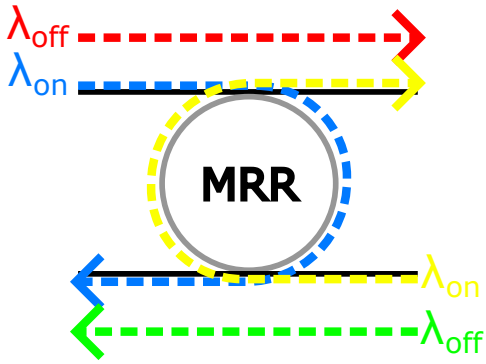

Figure 2.1.: PSE working mechanism.

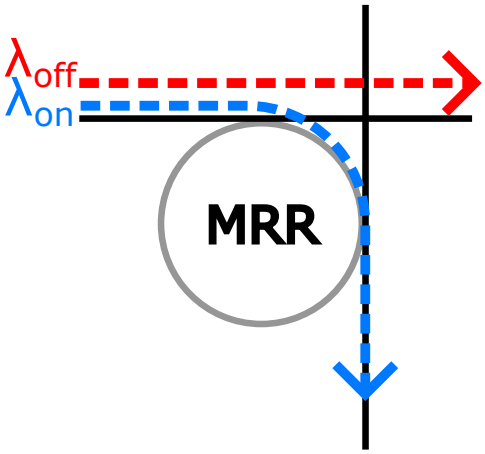

Figure 2.2.: 90° turns in CSEs.

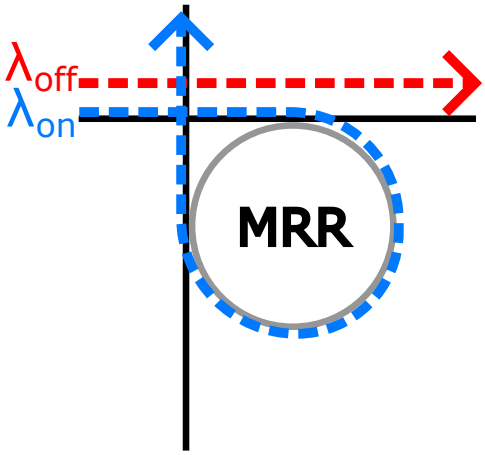

Figure 2.3.: 270° turns in CSEs.

Figure 2.4.: CSE working mechanism

power consumption and low latency characteristics make it highly suitable for application in WRONoCs.

Each input and output of GWOR is connected via specific waveguide channels. The smallest dimension of a GWOR topology is 4×4 in Figure 2.5, which consists of four CSEs. Its basic structure consists of a CSE with two identical MRRs, as shown in Figure 2.6. The even and odd wavelength assignment formulas for GWOR are as follows:

$$C(i,j)_{even} = \begin{cases} - & i = j \\ \lambda_{N-1} & i + j = N - 1, i \neq j \\ \lambda_{mod(2j,N-1)} & i = N - 1, \quad 0 < j < N - 1 \\ \lambda_{mod(N-1-2i,N-1)} & j = 0, \quad 0 < i < N - 1 \\ \lambda_{mod(j-i,N-1)} & \text{others} \end{cases} \tag{2.1}$$

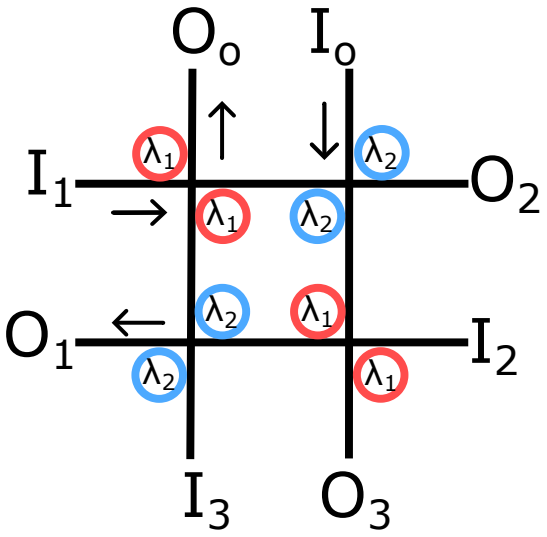

Figure 2.5.: 4×4 GWOR.

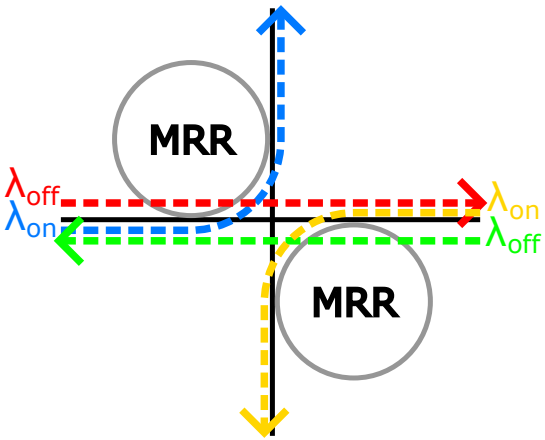

Figure 2.6.: A CSE with two MRRs.

$$C(i,j)_{odd} = \begin{cases} - & i = j \\ \lambda_{mod(j-i,N)} & \text{others} \end{cases} \tag{2.2}$$

These formulas can refer to a wavelength assignment table for GWOR of any dimension (X. Tan 2011). For example, the topological structures of an even-dimension 6×6 GWOR and an odd-dimension 7×7 GWOR are shown in Figure 2.7, and Figure 2.8, and their wavelength assignment tables are shown in Table 2.1 and Table 2.2.

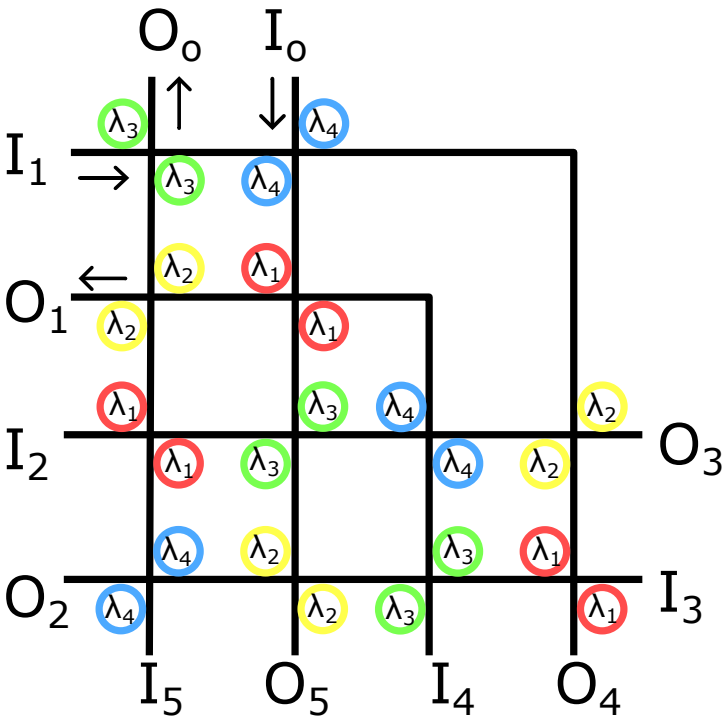

Figure 2.7.: 6×6 GWOR.

	O_0	O_1	O_2	O_3	O_4	O_5
I_0	-	λ_1	λ_2	λ_3	λ_4	λ_5
I_1	λ_3	-	λ_1	λ_2	λ_5	λ_4
I_2	λ_1	λ_4	-	λ_5	λ_2	λ_3
I_3	λ_4	λ_3	λ_5	-	λ_1	λ_2
I_4	λ_2	λ_5	λ_3	λ_4	-	λ_1
I_5	λ_5	λ_2	λ_4	λ_1	λ_3	-

Table 2.1.: 6×6 GWOR wavelength assignment.

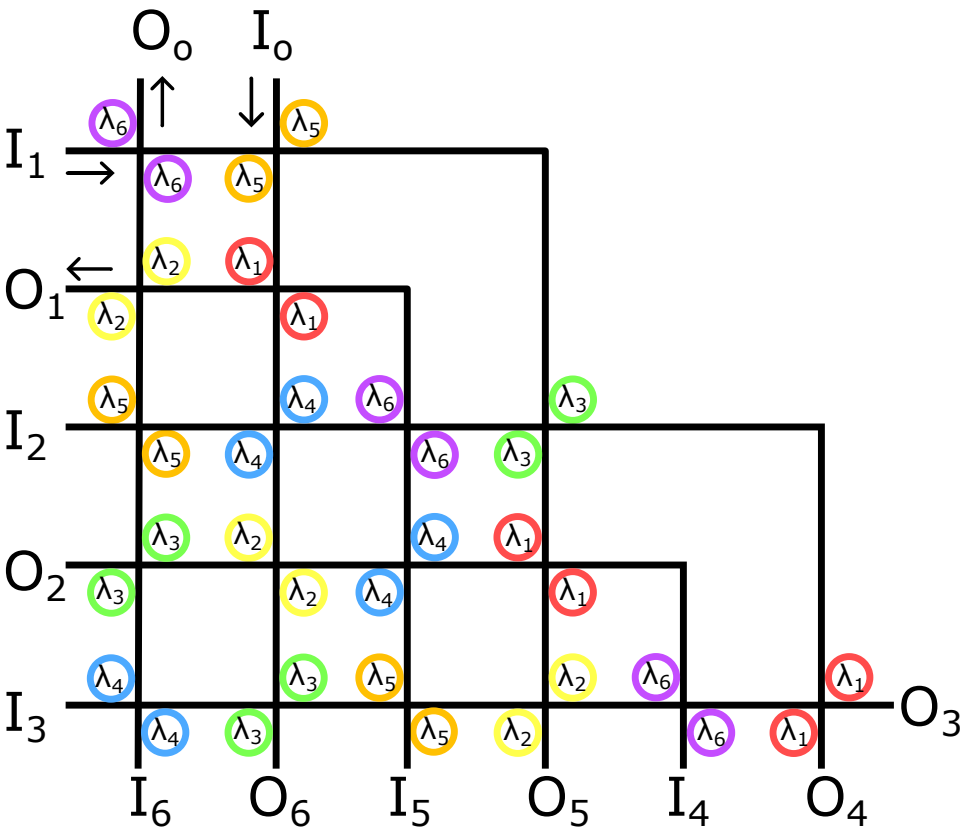

Figure 2.8.: 7×7 GWOR.

	O_0	O_1	O_2	O_3	O_4	O_5	O_6
I_0	-	λ_1	λ_2	λ_3	λ_4	λ_5	λ_6
I_1	λ_6	-	λ_1	λ_2	λ_3	λ_4	λ_5
I_2	λ_5	λ_6	-	λ_1	λ_2	λ_3	λ_4
I_3	λ_4	λ_5	λ_6	-	λ_1	λ_2	λ_3
I_4	λ_3	λ_4	λ_5	λ_6	-	λ_1	λ_2
I_5	λ_2	λ_3	λ_4	λ_5	λ_6	-	λ_1
I_6	λ_1	λ_2	λ_3	λ_4	λ_5	λ_6	-

Table 2.2.: 7×7 GWOR wavelength assignment.

2.4. Related work

M. Ortín et al. proposed strategies to partition a system and concurrently utilize multiple applications, emphasizing reusing wavelengths within each partition. Their experiments show that the strategies can effectively reduce static power consumption, the power of laser sources and improves power efficiency for photonically integrated systems (M. Ortin 2015). However, the strategy has three disadvantages:

First, the strategy still adopts a single topology, whose size is equal to the number of cores in the WRONoCs without reducing the size of the topology. The topology's dimensions determine the maximum usable wavelengths, and the insertion loss of a large-scale topology is higher than that of a small-scale one.

Second, the strategies do not consider insertion loss, a critical performance factor. Reducing wavelengths does not necessarily imply a reduction in insertion loss. When analyzing the insertion loss of each signal path in the topology, the insertion loss varies between the identical wavelengths. For example, in a 12×12 GWOR, the path wavelength assignment and insertion loss assignment are shown in Figure 2.3 and Figure 2.4. The insertion loss of wavelength λ_1 from I_0 to O_1 is 0.6 dB. However, the insertion loss of wavelength λ_1 from I_2 to O_3 is 1 dB. Reusing a wavelength without considering the increase in insertion loss can lead to high insertion loss, which increases the power consumption of the entire WRONoCs.

	O_0	O_1	O_2	O_3	O_4	O_5	O_6	O_7	O_8	O_9	O_{10}	O_{11}
I_0	-	1	2	3	4	5	6	7	8	9	10	11
I_1	9	-	1	2	3	4	5	6	7	8	11	10
I_2	7	10	-	1	2	3	4	5	6	11	8	9
I_3	5	9	10	-	1	2	3	4	11	6	7	8
I_4	3	8	9	10	-	1	2	11	4	5	6	7
I_5	1	7	8	9	10	-	11	2	3	4	5	6
I_6	10	6	7	8	9	11	-	1	2	3	4	5
I_7	8	5	6	7	11	9	10	-	1	2	3	4
I_8	6	4	5	11	7	8	9	10	-	1	2	3
I_9	4	3	11	5	6	7	8	9	10	-	1	2
I_{10}	2	11	3	4	5	6	7	8	9	10	-	1
I_{11}	11	2	4	6	8	10	1	3	5	7	9	-

Table 2.3.: 12×12 GWOR wavelength assignment.

(dB)	O_0	O_1	O_2	O_3	O_4	O_5	O_6	O_7	O_8	O_9	O_{10}	O_{11}
I_0	-	0.6	0.7	0.8	0.9	1	1.3	1.2	1.1	1	0.9	0.5
I_1	0.5	-	0.8	0.9	1	1.1	1.2	1.1	1	0.9	0.5	1
I_2	0.6	0.7	-	1	1.1	1.2	1.1	1	0.9	0.5	1	0.9
I_3	0.7	0.8	0.9	-	1.2	1.3	1	0.9	0.5	1	0.9	0.8
I_4	0.8	0.9	1	1.1	-	1.4	0.9	0.5	1	0.9	0.8	0.7
I_5	0.9	1	1.1	1.2	1.3	-	0.5	1	0.9	0.8	0.7	0.6
I_6	1.4	1.3	1.2	1.1	1	0.5	-	0.5	0.6	0.7	0.8	0.9
I_7	1.3	1.2	1.1	1	0.5	0.9	0.6	-	0.7	0.8	0.9	1
I_8	1.2	1.1	1	0.5	0.9	0.8	0.7	0.8	-	0.9	1	1.1
I_9	1.1	1	0.5	0.9	0.8	0.7	0.8	0.9	1	-	1.1	1.2
I_{10}	1	0.5	0.9	0.8	0.7	0.6	0.9	1	1.1	1.2	-	1.3
I_{11}	0.5	0.9	0.8	0.7	0.6	0.5	1	1.1	1.2	1.3	1.4	-

Table 2.4.: 12×12 GWOR insertion loss.

2.5. Typical partitioning methods

Two classical partitioning methods will be introduced, which can fit the demands of reducing the communication between partitions and minimizing the maximum partition size during WRONoCs partitioning.

2.5.1. Kernighan-Lin Algorithm

The Kernighan-Lin algorithm, often used to minimize inter-board connections in electronic circuits, can also partition ONoC's communication. This algorithm offers two methods: even partitioning and uneven partitioning.

First, the even partitioning problem can evenly divide the input graph into two equal-sized subsets while minimizing the total edge weight between the two subsets. The method requires that the number of nodes in the graph be even to ensure a fundamental equal division.

The second method involves uneven partitioning. The method requires the sizes of the two subsets in advance. By continuously exchanging nodes between the two subsets until all nodes have been exchanged once, two subsets with the minimum total edge weight between them are obtained (B. W. Kernighan 1970).

The Kernighan-Lin algorithm can halve the maximum topology size in WRONoCs and minimize the edges between partitions, meaning fewer communications are inter-partitions. The topology size of inter-partitions can also be effectively controlled. However, for the algorithm of evenly dividing into two subsets, the size of the topology must be even to partition. Predefined partition sizes are necessary for uneven partitioning, which can limit the algorithm's flexibility and practical applicability. A characteristic of both methods is that they can only divide the graph into two sub-graphs but not into multiple sub-graphs. Therefore, these methods are highly effective in decreasing the maximal partitions' size with small-scale graphs but less effective for large-scale graphs.

2.5.2. Stoer-Wagner Minimum Cut Algorithms

The Stoer-Wagner minimum cut algorithm aims to divide a graph into two parts so that the total weight of the cut is minimized. The Stoer-Wagner minimum cut algorithm finds the minimum cut by contracting vertices in phases (F. Wagner 1997).

The Stoer-Wagner minimum cut algorithm effectively controls the inter-partition cut's size and ensures reduced communication between the partitions. However, while the minimum cut algorithm can minimize the cut, but it can not control the size of the partitions, which often results in significant size disparities between partitions.

3. Preliminaries

The maximum insertion loss generated on the signal paths and the overall number of wavelengths used significantly influence the total laser power (M. Ortín-Obón 2017). These two parameters will be essential reference variables in the subsequent work.

3.1. Calculation of insertion loss

The insertion loss for each signal path can be calculated based on the number of MRRs each signal passes through and the number of resonances that occur.

When an input signal passes through an MRR without being coupled to the MRR, it generates a through signal loss(L_t). When the signal is coupled to the MRR, a drop loss(L_d) is generated. A crossing loss(L_c) is incurred when a signal passes through a waveguide crossing. Tablet 3.1 shows the insertion loss coefficients of them (M. Nikdast 2015). The physical structure of the GWOR leads to variations in the number of MRRs each signal path traverses and the instances of resonance. Using a GWOR with a dimension of 7 as an example in Figure 2.8, analyze the insertion loss on the path from I_0 to I_6 in Figure 3.1 and from I_2 to O_5 in Figure 3.2. By calculating the number of MRRs each signal path passes through ($N_{Through}$), the number of CSE passes through ($N_{Crossing}$), the number of resonances (N_{Drop}, which is 1 or 0 in GWOR) occurred on the signal path, the insertion loss generated on these two paths can be caculated.

First, Figure 3.2 shows an example where the input signal starts from I_0, and for each MRR it passes through, $N_{Through}$ increases by one, resulting in $N_{Through}$ being 10. Similarly, $N_{Crossing}$ increases by one for each crossing, resulting in $N_{Crossing}$ being 5. By referring to the wavelength assignment Tablet 2.2, the resonance wavelength of the signal from I_0 to O_6 is λ_6. However, no MRR on the path with a resonance wavelength is λ_6, N_{Drop} is 0. The total insertion losses can be calculated according to Formula 3.1. The insertion loss of the signal from I_0 to O_6 is calculated as follows:

$$IL = |L_t| \times N_{Through} + |L_c| \times N_{Crossing} + |L_d| \times N_{Drop} \tag{3.1}$$

Through loss (L_t)	Drop loss (L_d)	Crossing loss (L_c)
0.005 dB	0.5 dB	0.04 dB

Table 3.1.: Insertion loss coefficients.

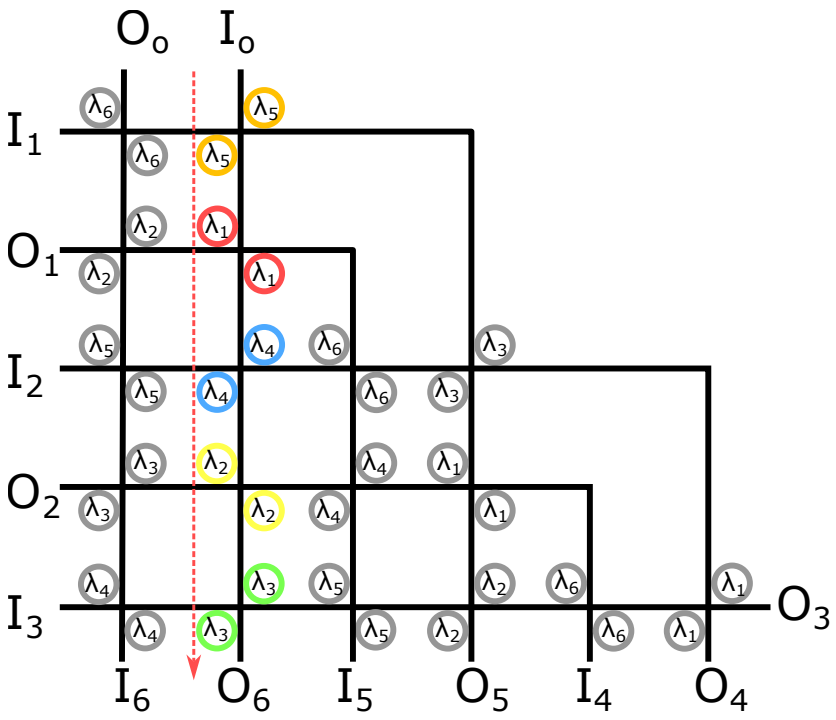

Figure 3.1.: Signal path from I_0 to O_6.

$$\begin{aligned} Loss_{I_0 \to O_6} &= 0.005 \times N_{Through} + 0.04 \times N_{Crossing} + 0.5 \times N_{Drop} \\ &= 0.005 \times 10 + 0.04 \times 5 + 0.5 \times 0 \\ &= 0.25 \end{aligned}$$

Second, for another example, the resonance wavelength from I_2 to O_5 is λ_3. When the signal encounters the MRR with resonance wavelength of λ_3, it passes with a 90° transmission change, and N_{Drop} is 1. For the remaining MRRs and CSEs, $N_{Through}$ is 10, and $N_{Crossing}$ is 5. The insertion loss of the signal from I_2 to O_5 is calculated as follows:

$$\begin{aligned} Loss_{I_2 \to O_5} &= 0.005 \times N_{Through} + 0.04 \times N_{Crossing} + 0.5 \times N_{Drop} \\ &= 0.005 \times 10 + 0.04 \times 5 + 0.5 \times 1 \\ &= 0.75 \end{aligned}$$

Following the same process, a table for the insertion loss of a 7×7 GWOR, as shown in Tablet 3.2, can be caculated.

With the method described above, the insertion loss of the physical topology of the GWOR in odd dimensions can be derived. Equation 3.3 shows the number of crossings that pass through on each path, where N is the dimension of GWOR, i is the input port number, and j is the output port number. For GWORs of even dimensions, calculate and analyze the signal

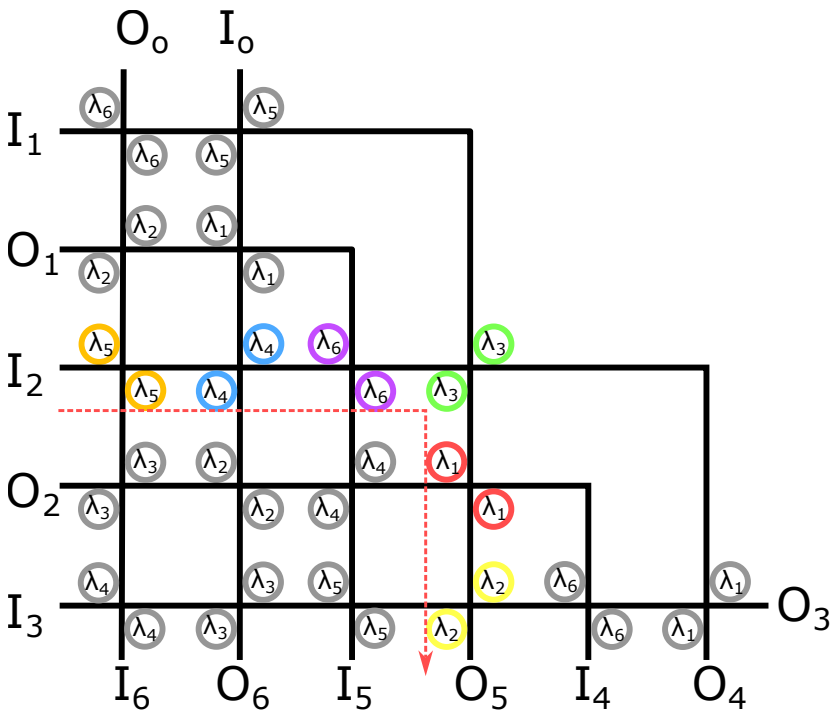

Figure 3.2.: Signal path from I_2 to O_5.

path insertion loss similarly. The number of crossings that pass through on each path for the GWOR in the even dimension is presented in Equation 3.2.

The relationship between the number of crossings and the number of MRRs a signal passes through is given by Equation 3.4. The number of resonances occurring on the signal path is shown in Equation 3.5.

(dB)	O_0	O_1	O_2	O_3	O_4	O_5	O_6
I_0	-	0.6	0.7	0.9	0.75	0.65	0.25
I_1	0.5	-	0.8	0.8	0.65	0.25	0.75
I_2	0.6	0.7	-	0.7	0.25	0.75	0.65
I_3	0.7	0.8	0.9	-	0.75	0.65	0.55
I_4	0.85	0.75	0.25	0.55	-	0.6	0.7
I_5	0.75	0.25	0.65	0.65	0.7	-	0.8
I_6	0.25	0.65	0.55	0.75	0.8	0.9	-

Table 3.2.: 7×7 GWOR insertion loss.

$$N_{crossing\_odd}(i,j) = \begin{cases} 0 & i = j \\ N-2 & i+j = N-1, \quad i \neq j \\ 2(N-3)-2i & j = \frac{N-1}{2}, \quad 0 \leq i < \frac{N-1}{2} \\ 2i-N & j = \frac{N-1}{2}, \quad \frac{N-1}{2} < i < N \\ 2(i-1)+2j & 0 < i \leq \frac{N-1}{2}, \quad i > j \\ 2(i+j) & 0 < j < \frac{N-1}{2}, \quad i < j \\ (3N-8)-2(i+j) & \frac{N-1}{2} < j < N, \quad i+j < N-1 \\ (3N-2)-2(i+j) & 0 < i \leq \frac{N-1}{2}, \quad i+j > N-1 \\ (3N-6)-2(i+j) & \frac{N-1}{2} < i < N-1, \quad i+j < N-1 \\ (3N-4)-2(i+j) & 0 < j < \frac{N-1}{2}, \quad i+j > N-1 \\ 2(i+j)-2N & \frac{N-1}{2} < j < N-1, \quad i > j \\ 2(i+j)-2(N+1) & \frac{N-1}{2} < i < N-1, \quad i < j \end{cases} \tag{3.2}$$

$$N_{crossing\_even}(i,j) = \begin{cases} 0 & i = j \\ N-2 & i+j = N-1, \quad i \neq j \\ 2(i-\frac{N}{2}) & \frac{N}{2} < i < N, \quad j = \frac{N}{2} \\ 2(i-1)+2j & 0 < i < \frac{N}{2}, \quad i > j \\ 2(i+j) & 0 < j < \frac{N}{2}, \quad i < j \\ (3N-8)-2(i+j) & \frac{N}{2} \leq j < N, \quad i+j < N-1 \\ (3N-2)-2(i+j) & 0 < i < \frac{N}{2}, \quad i+j > N-1 \\ (3N-6)-2(i+j) & \frac{N}{2} \leq i < N-1, \quad i+j < N-1 \\ (3N-4)-2(i+j) & 0 < j < \frac{N}{2}, \quad i+j > N-1 \\ 2(i+j)-2N & \frac{N}{2} < j < N, \quad i > j \\ 2(i+j)-2(N-1) & \frac{N}{2} \leq i < N, \quad i < j \end{cases} \tag{3.3}$$

$$N_{through}(i,j) = 2 \times N_{crossing}(i,j) \tag{3.4}$$

$$N_{drop}(i,j) = \begin{cases} 0 & i = j \\ 0 & i+j = N-1, \quad i \neq j \\ 1 & \text{others} \end{cases} \tag{3.5}$$

(dB)	O_0	O_1	O_2	O_3	O_4	O_5	O_6	O_7	O_8	O_9	O_{10}	O_{11}	O_{12}	O_{13}	O_{14}	O_{15}
I_0	-	0.6	0.7	0.8	0.9	1	1.1	1.2	1.7	1.6	1.5	1.4	1.3	1.2	1.1	0.7
I_1	0.5	-	0.8	0.9	1	1.1	1.2	1.3	1.6	1.5	1.4	1.3	1.2	1.1	0.7	1.2
I_2	0.6	0.7	-	1	1.1	1.2	1.3	1.4	1.5	1.4	1.3	1.2	1.1	0.7	1.2	1.1
I_3	0.7	0.8	0.9	-	1.2	1.3	1.4	1.5	1.4	1.3	1.2	1.1	0.7	1.2	1.1	1
I_4	0.8	0.9	1	1.1	-	1.4	1.5	1.6	1.3	1.2	1.1	0.7	1.2	1.1	1	0.9
I_5	0.9	1	1.1	1.2	1.3	-	1.6	1.7	1.2	1.1	0.7	1.2	1.1	1	0.9	0.8
I_6	1	1.1	1.2	1.3	1.4	1.5	-	1.8	1.1	0.7	1.2	1.1	1	0.9	0.8	0.7
I_7	1.1	1.2	1.3	1.4	1.5	1.6	1.7	-	0.7	1.2	1.1	1	0.9	0.8	0.7	0.6
I_8	1.8	1.7	1.6	1.5	1.4	1.3	1.2	0.7	-	0.5	0.6	0.7	0.8	0.9	1	1.1
I_9	1.7	1.6	1.5	1.4	1.3	1.2	0.7	1.1	0.6	-	0.7	0.8	0.9	1	1.1	1.2
I_{10}	1.6	1.5	1.4	1.3	1.2	0.7	1.1	1	0.7	0.8	-	0.9	1	1.1	1.2	1.3
I_{11}	1.5	1.4	1.3	1.2	0.7	1.1	1	0.9	0.8	0.9	1	-	1.1	1.2	1.3	1.4
I_{12}	1.4	1.3	1.2	0.7	1.1	1	0.9	0.8	0.9	1	1.1	1.2	-	1.3	1.4	1.5
I_{13}	1.3	1.2	0.7	1.1	1	0.9	0.8	0.7	1	1.1	1.2	1.3	1.4	-	1.5	1.6
I_{14}	1.2	0.7	1.1	1	0.9	0.8	0.7	0.6	1.1	1.2	1.3	1.4	1.5	1.6	-	1.7
I_{15}	0.7	1.1	1	0.9	0.8	0.7	0.6	0.5	1.2	1.3	1.4	1.5	1.6	1.7	1.8	-

Table 3.3.: 16×16 GWOR insertion loss.

Dimension	7	16
Maximum Insertion Loss	0.9 dB	1.8 dB
Minimum Insertion Loss	0.25 dB	0.5 dB

Table 3.4.: Comparison of maximum insertion loss of two different dimension GWOR.

Based on the aforementioned formula, the insertion loss of any size GWOR is scalable.

After calculating the insertion loss for a 16×16 GWOR topology, as shown in Table 3.3, compare the maximum and minimum insertion loss for a 16-dimensional GWOR with a 7-dimensional GWOR in Table 2.2. According to the results in Table 3.4, it can be inferred that the maximum insertion loss increases with the increase of topology dimension.

3.2. Insertion loss within different clusters

Dividing a core graph, i.e., a communication network with many cores, into different clusters needs an additional topology to enable communication between clusters. The clustering method will be introduced in the next section. This section will introduce how to achieve inter-cluster communication and how to calculate the corresponding insertion loss.

The signal inter-clusters cannot be directly supported like the nodes inside the clusters by a topology; instead, an additional MRR is necessary to connect the communication of each node to the topology, which is dedicated to supporting inter-cluster communication. The core

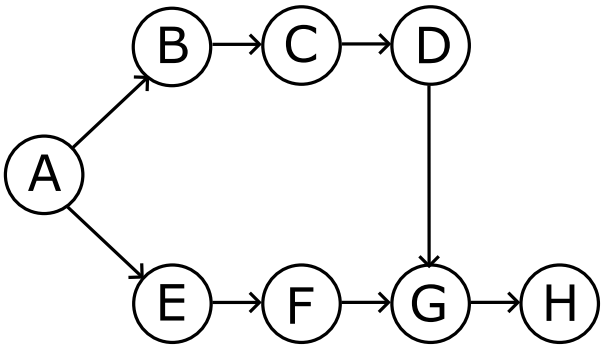

Figure 3.3.: PIP core graph. Each node represents a core.

graph of $Picture - In - Picture$ (PIP), which is a video processing application on NetChip, is mapped onto 8 cores and shown in Figure 3.3 (D. Bertozzi 2005). To analyze the connection inter-clusters, I cluster the PIP core graph with my method and support each cluster with the corresponding dimensional topology. Figure 3.4 presents the communications of the intra- and inter-clusters in the PIP core graph. The connections between the intra-clusters and inter-cluster of their topologies are illustrated in Figure 3.5. The topological connections in the figure correspond to the clustering and topology pairing depicted in Figure 3.4. Figure 3.5 shows three 4×4 GWOR topologies corresponding to intra-cluster 1, intra-cluster 2, and the inter-cluster topology.

Therefore, for the topology of inter-cluster, except the insertion loss that generates inside the topology, an additional drop loss (L_d) generated by the additional MRR must be added to obtain the total insertion loss produced by the inter-cluster's topology. Given that 0.5 dB is two orders of magnitude greater than L_t and one order of magnitude greater than L_c, appropriately control the number of inter-cluster cores during clustering to prevent excessive dimensions and insertion loss in the topology.

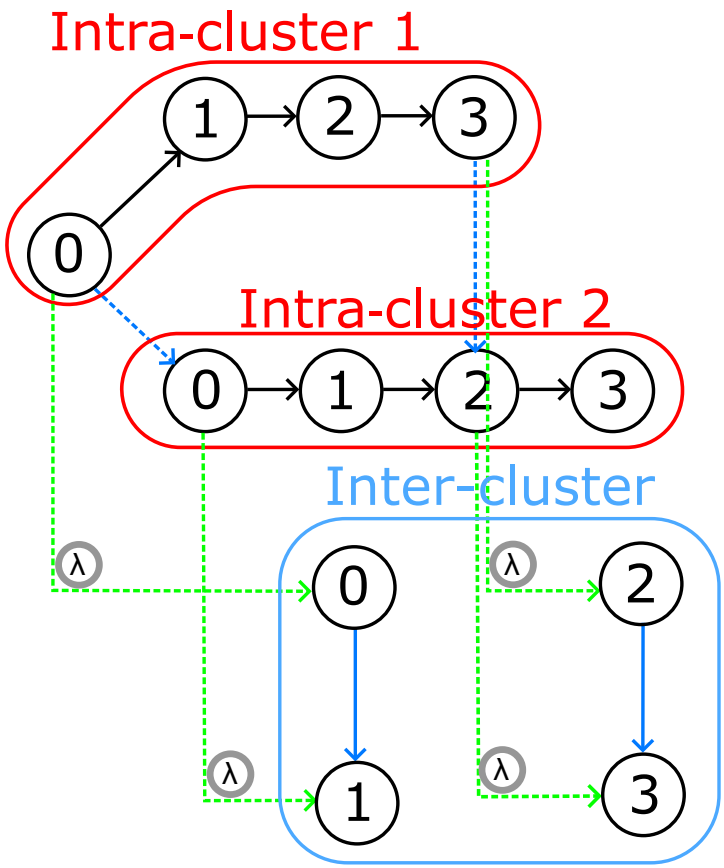

Figure 3.4.: Intra- and inter-clusters communication graph of PIP core graph. The numbers of each node are the input and output ports' index of the topologies supporting the clusters. The red sections and the blue section represent the intra-clusters and the inter-cluster. The blue lines represent the inter-cluster's signal communication. The gray MRRs indicate the MRRs required for connecting inter-cluster signals, and the green arrows represent waveguides.

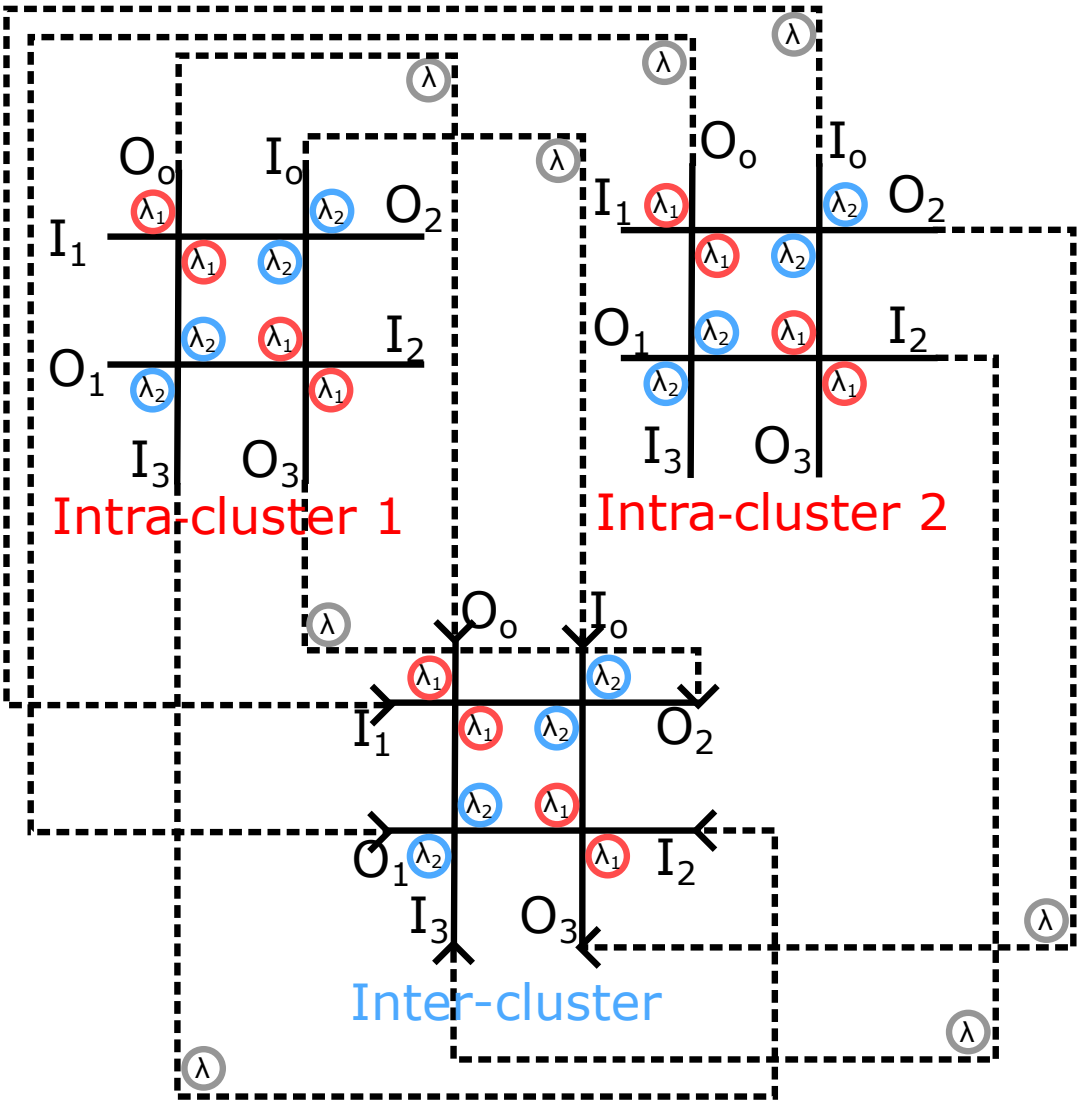

Figure 3.5.: Connections between the intra- and inter-clusters of the topologies.

4. Methodology

4.1. Clustering Method

Most partitioning algorithms struggle to divide a directed graph into more than two partitions. Some partitioning algorithms that support multiple partitions still require a predefined number of partitions. Predicting the number of partitions needed to minimize the maximum insertion loss of the entire network is challenging. This work proposes a clustering-based algorithm that relies on the inherent connectivity between nodes in the directed graph to address the issue of predefining the number of partitions.

To simplify the analysis of communication networks on WRONoCs, transform the communication networks into directed graphs based on concepts from graph theory, referred to in this work as the core graph. Each node on the core graph represents a core. The neighbors of a core represent its adjacent nodes. The edges of a core are the connections between the core and its neighbors. The degree of a core represents the number of edges of the core.

My clustering algorithm begins by selecting a node with the highest degree as the starting node and merges it with its lower-degree neighbors. A high-degree node indicates that the node has many neighbors. Low-degree neighbors of the high-degree node imply that the connections between the high-degree node and its lower-degree neighbors are relatively tighter than others with higher-degree neighbors. For example, the core graph for a video processing application MPEG4 is shown in Figure 4.1 (D. Bertozzi 2005). Node E with the highest degree in the core graph has a degree of 14 and has 7 neighbors. The neighbors with the lowest degree are nodes A, B, and I, while those with the highest degree are nodes C, D, J, and K. Unlike node A, node C, besides being closely connected to node E, is also closely related to node F. If node E merges with its lower-degree neighbors, the degree of the new cluster will reduce compared to the unmerged cluster. For instance, when node E is merged with the lowest-degree node B, the merged cluster has 12 degrees. However, if node E merges with a higher-degree node like node C, the degree of the merged cluster is still 14. The process is shown in Figure 4.2(a) and Figure 4.2(b).

The choice of stopping conditions greatly affects the final results, and stopping conditions can be adjusted according to different evaluation conditions. Set a variable L to assess cluster quality, where

$$L = 0.5 \cdot N_{WL} + 5 \cdot IL_{max}$$

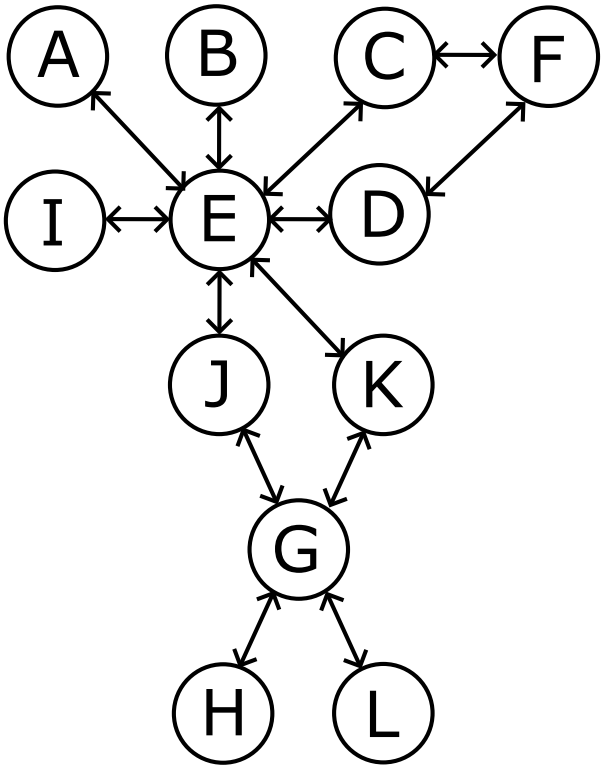

Figure 4.1.: MPEG4 core graph.

N_{WL} represents the number of wavelengths and IL_{max} represents the maximum insertion loss. The coefficient for N_{WL} was set to 0.5, and the coefficient for IL_{max} was chosen as 5 to balance the values of these two metrics based on their magnitudes. However, in practical applications, the coefficients can be adjusted according to the relative weight of each parameter. A threshold N is introduced to prevent the process from stopping prematurely due to a temporary increase in L or the edges of inter-cluster when the number of nodes in a cluster increases.

The clustering algorithm has three main steps:

Input: core graph, threshold N

1. Identify the node with the highest degree in the graph:

   a. If there is only one node, select it as the start node.

   b. If there are multiple nodes with the highest degree, select the node with the smallest sum of the degrees of its neighbors.

   c. If multiple nodes have the same highest degree and the identical sum of neighbor degrees, select the smallest cluster/node.

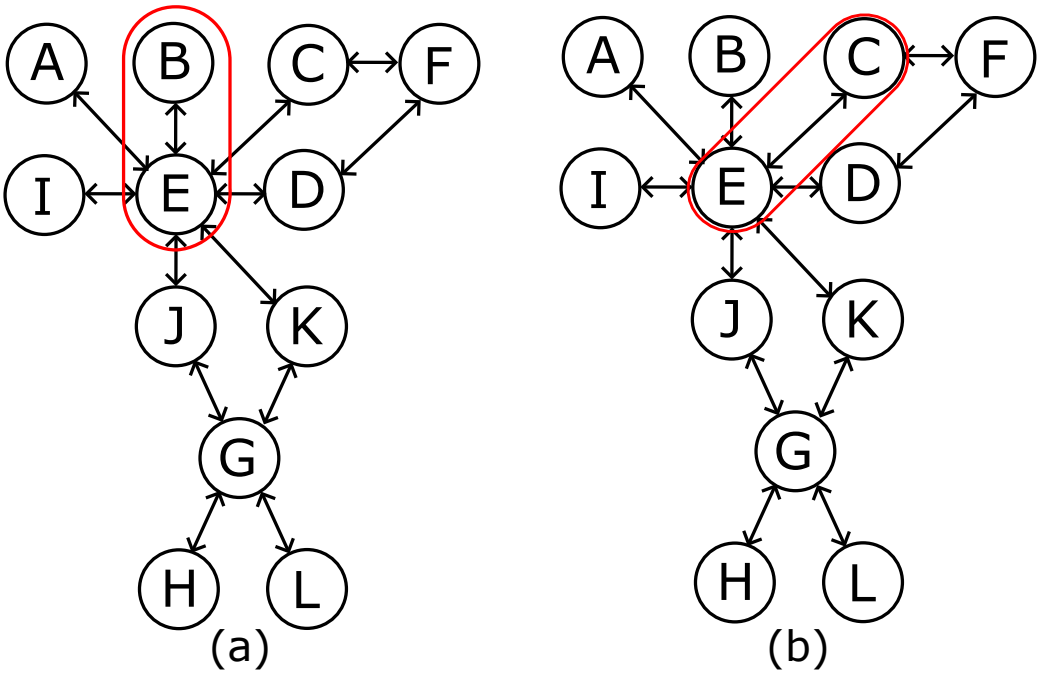

Figure 4.2.: (a) Merge node E with node B. (b) Merge node E with node B.

d. Otherwise, choose the candidate nodes randomly

2. Merge this start node with its neighbor, treating the entire cluster as a merged cluster/node:

a. Only one neighbor that results in the largest reduction in the degree of the merged cluster/node.

b. Multiple neighbors that each result in the largest reduction in the degree. Select the one with the lowest degree.

c. Multiple neighbors that each result in the largest reduction in the degree. If their degrees are the same, choose the one with the smallest cluster size.

d. Multiple neighbors each result in the largest reduction in the degree; if the degrees are the same and the size of clusters are the same, select the neighbor with the smallest sum of the degrees of its neighbors.

e. Otherwise, choose the candidate nodes randomly

3. After each merging, calculate the core graph's maximum insertion loss and wavelength usage. If the stopping condition is not reached, return to step one.

Based on the previous analysis of the factors influencing the WRONoCs, I established the

following stopping conditions:

a. Stop after the total edges of the inter-cluster increase by N times, where N is the threshold for times of the inter-cluster edges increase.

b. Stop after L increases N times, where L is the evaluation value of the entire clustered network.

Output: The final result is the clustering method that results in the minimum L throughout the process.

4.2. Node-Pairing Methods

To support all the cores on WRONoCs with topology, each node on the core graph must be paired with the topology's input and output ports. A reasonable node pairing can significantly improve the maximum insertion loss of the entire network. For example, using an 8-core graph as an example, the PIP core graph in Figure 3.3, the maximum insertion loss and wavelength assignment are different with the same topology, but with a different node pairing sequence. The 8×8 insertion loss assignment of each path is shown in Tablet A.1 in appendix. Figure 4.3 shows the maximum insertion loss and wavelength assignment of the PIP core graph with randomly paired nodes. In contrast, Figure 4.4 displays the insertion loss and wavelength assignment after minimizing the maximum insertion loss of the entire network. Node's numbers on the node in the figure represent the pairing topology's input and output ports. The comparison in Table 4.1 demonstrates that the maximum insertion loss of the PIP core graph is decreased by 0.3 dB.

To minimize the maximum insertion loss of WRONoCs, selecting paths with minimal insertion loss is crucial when pairing nodes. When selecting paths, the rules that all input signals from a core must have different wavelengths and that all output signals must also have different wavelengths should strictly follow. The following sections will introduce two node-pairing methods.

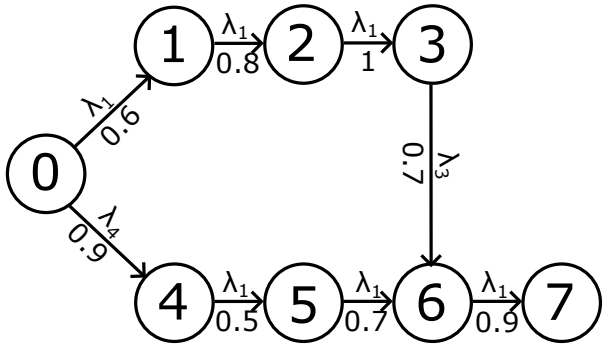

Figure 4.3.: Insertion loss and wavelength assignment of PIP communication graph with pairing the node randomly.

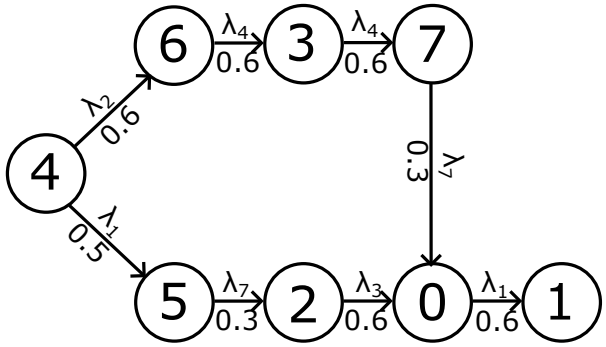

Figure 4.4.: Insertion loss and wavelength assignment of PIP communication graph with node pairing minimizing the maximum insertion loss.

	Maximum Insertion Loss
Pairing nodes randomly	0.9 dB
Pairing nodes with minimizing the maximum insertion loss	0.6 dB

Table 4.1.: Comparison of maximum insertion loss and wavelength usage of PIP core graph.

4.2.1. Exhausted Searching Method

The exhausted searching method is the most straightforward approach, as it involves pairing every node in the core graph with each input and output port in the topology and finding the pairing that minimizes the maximum insertion loss. However, it has a high computational complexity and long execution time, exspecifically when the topology dimension is large. The computational workload grows factorially with the sizes of core graphs. Nevertheless, as the method is guaranteed to find the optimal node pairing, it remains effective when the number of nodes within a partition is relatively small.

4.2.2. Random Shuffling Method

Randomly shuffle all possible node-pairing scenarios and select the first N_{sample} for insertion loss evaluation. N_{sample} represents the sample size, and its value depends on the topology size and the acceptable execution time. The output is the node pairing scenario, resulting in the minimal maximum insertion loss within the samples. This method can find a relatively small maximum insertion loss. However, when the dimension of core graphs is large, this method will likely find only a relatively local minimum value rather than the global minimum value.

5. Results

I compared the clustering methods mentioned above with several applications to analyze the clustering methods. All core graphs used in this study are shown in the appendix in Figures 3.3, 4.1, 1.1(a), A.4 (D. Bertozzi 2005), and A.5 (C. Seiculescu 2009). I implemented my clustering method and the other approaches in Python. The Python scripts utilized standard libraries, such as NumPy for numerical computations, NetworkX for graph operations, etc. The experiments were conducted on a Laptop equipped with an AMD Ryzen 7 6800H CPU running at 3201 MHz. The comparison below analyzes the maximum insertion loss and wavelength usage between my clustering method and conventional methods, as well as between the two partitioning methods. After clustering, I discussed the computation times of the two node-pairing methods and their performance in reducing insertion loss and wavelength usage.

5.1. Comparison to a conventional method

As shown in Figures 5.1, 5.2, 5.3, 5.4, and 5.5 illustrate all core graphs after applying all three clustering methods for dividing effectively the PIP core graph, the MPEG4 core graph, the VOPD core graph, the MWD core graph and the D-26-media core graph, into multiple sub-graphs. Tablet 5.1 and Tablet 5.2 respectively show the wavelength usage and the maximum insertion loss of all the core graphs.

Specifically, compared to the other core graphs, the PIP core graph using a single GWOR has lower insertion loss and wavelength usage than after clustering. Because the PIP core graph only has eight cores, and for an 8×8 GWOR, the maximum insertion loss is 1 dB, shown in Tablet A.1 in the appendix. The minimum dimension for GWOR is 4, with a maximum insertion loss of 0.6 dB. However, after clustering the 8-core graph, the maximum inter-cluster insertion loss increases by 0.5 dB due to the additional MRRs. Therefore, the maximum insertion loss after clustering into two clusters easily exceeds 1 dB. Based on this example, it can be inferred that when the number of cores is less than or equal to eight, using a single topology for routing is more optical than clustering.

$N_{wavelength}$	PIP	MPEG4	VOPD	MWD	D-26-media
A single topology	3	10	9	6	19
Kernighan-Lin	3	8	3	6	8
Stoer-Wagner minimum cut	4	11	10	6	17
My method	3	8	4	3	9

Table 5.1.: Wavelength usage results for various applications.

IL_{max} (dB)	PIP	MPEG4	VOPD	MWD	D-26-media
A single topology	1	1.3	1.4	1.3	2.4
Kernighan-Lin	0.6	1.1	1.1	1.1	1.4
Stoer-Wagner minimum cut	1	1.1	1.3	1.2	2.7
My method	0.6	1.1	0.6	0.65	1.1

Table 5.2.: Maximum insertion loss results for various applications.

5.2. Comparison to typical partitioning algorithms

According the results in Tablet 5.1 and Tablet 5.2, Kernighan-Lin algorithm can reduce wavelength usage and maximum insertion loss compared to the conventional method. However, the Kernighan-Lin algorithm results in some nodes in intra-partitions having no communication with other nodes. Take the VOPD core graph 5.3(a) as an example: it is evident that node A and node B were forced into the red partition to balance the partition sizes, which compromises the partition quality, leading to higher insertion loss than my method.

The Stoer-Wagner minimum cut algorithm easily partitioned cores with only one neighbor into a single partition due to the lack of constraints over the sizes of the two partitions. For example, the single node H in Figure 5.3(b) is a partition. The Stoer-Wagner minimum cut algorithm only minimizes the cut between the inter-partitions. However, the scale of the maximal partition is still significant. This results in higher maximum insertion loss and wavelength usage than my method and the Kernighan-Lin algorithm.

Since the Kernighan-Lin algorithm and the Stoer-Wagner minimum cut algorithm can only divide the network into two partitions, they can not effectively reduce the largest partition size for relatively large-scale graphs. Compared with it, my method does not constrain the number of clusters. The core graph's connectivity and stop conditions primarily determine my method's clustering. For example, with the VOPD core graph in Figure 5.3(c), my method divided the core graph into three clusters of size 4. The VOPD core graph in Figure 5.3(a) is divided into two clusters of size 6. The size of the maximal cluster divided by my method in the VOPD core graph is smaller than that of the Kernighan-Lin algorithm and the Stoer-Wagner minimum cut algorithm, which also reduces the maximum insertion loss and wavelength usage.

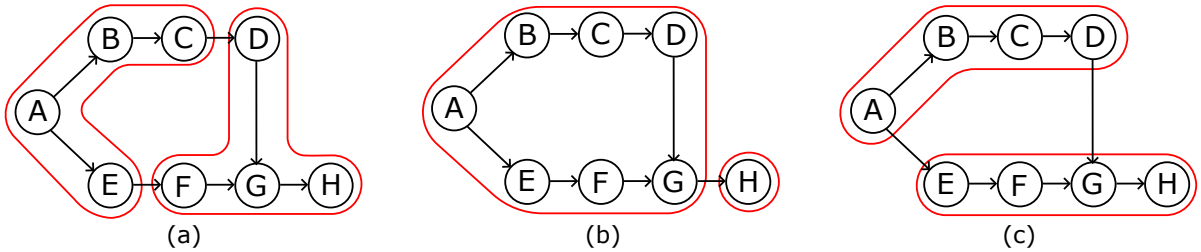

Figure 5.1.: Partitioning results of PIP core graph using (a) Kernighan-Lin, (b) Stoer-Wagner minimum cut, and (c) My method

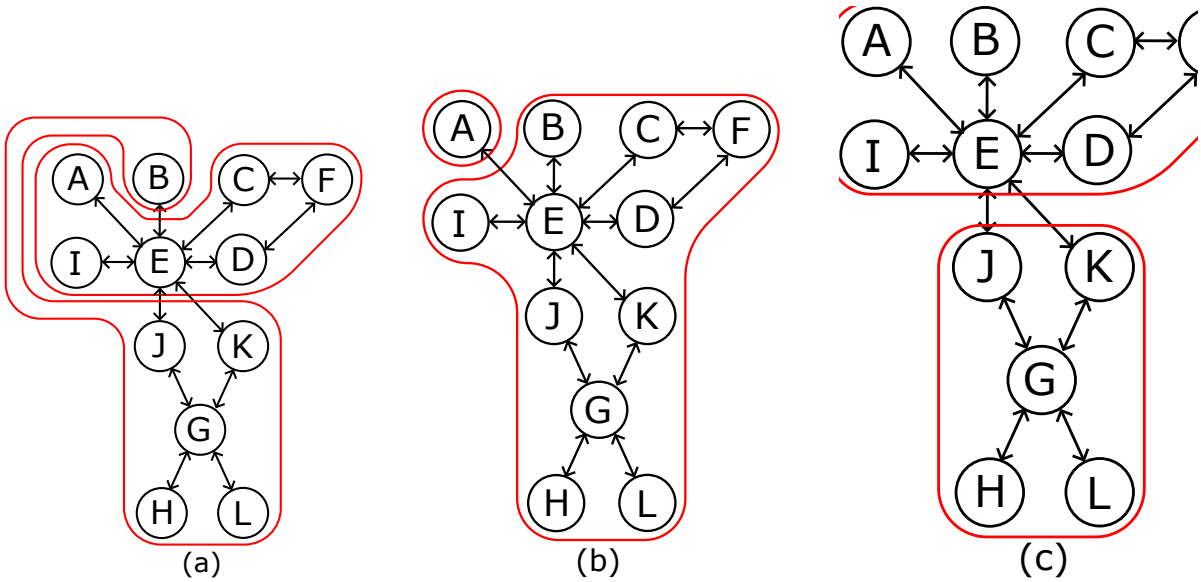

Figure 5.2.: Partitioning results of MPEG4 core graph using (a) Kernighan-Lin, (b) Stoer-Wagner minimum cut, and (c) My method

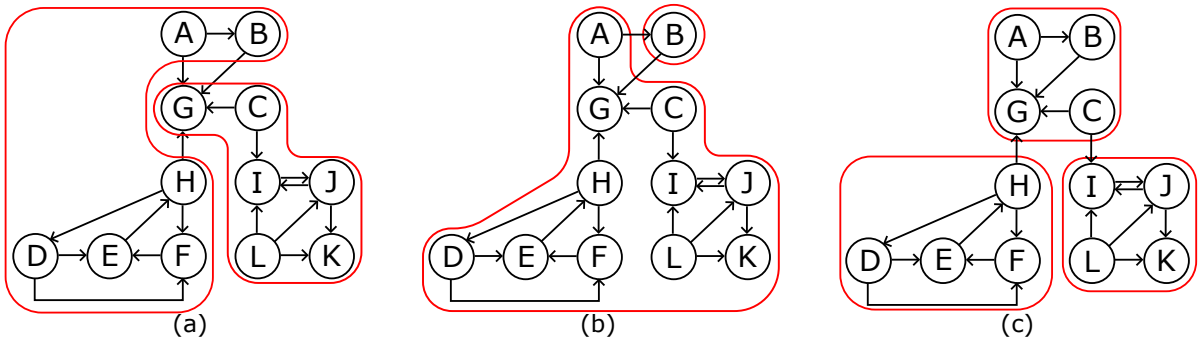

Figure 5.3.: Partitioning results of VOPD core graph using (a) Kernighan-Lin, (b) Stoer-Wagner minimum cut, and (c) My method.

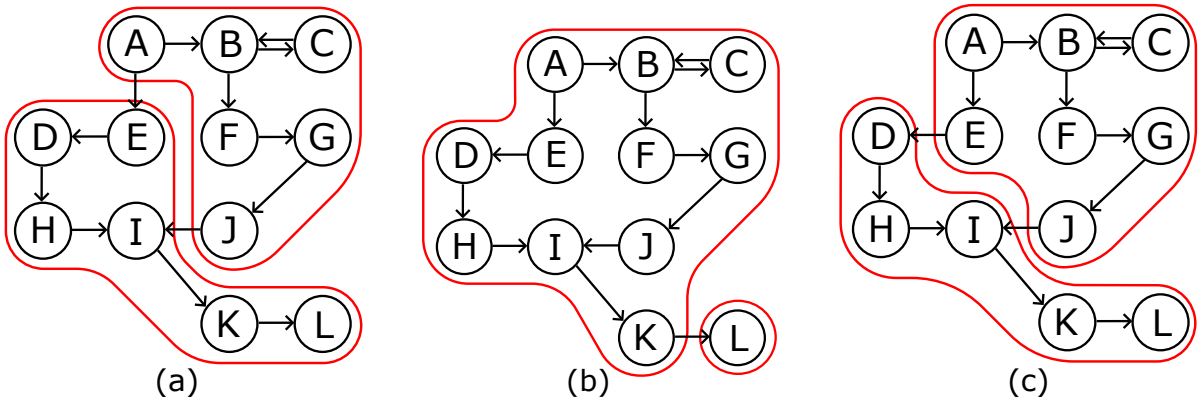

Figure 5.4.: Partitioning results of MWD core graph using (a) Kernighan-Lin, (b) Stoer-Wagner minimum cut, and (c) My method.

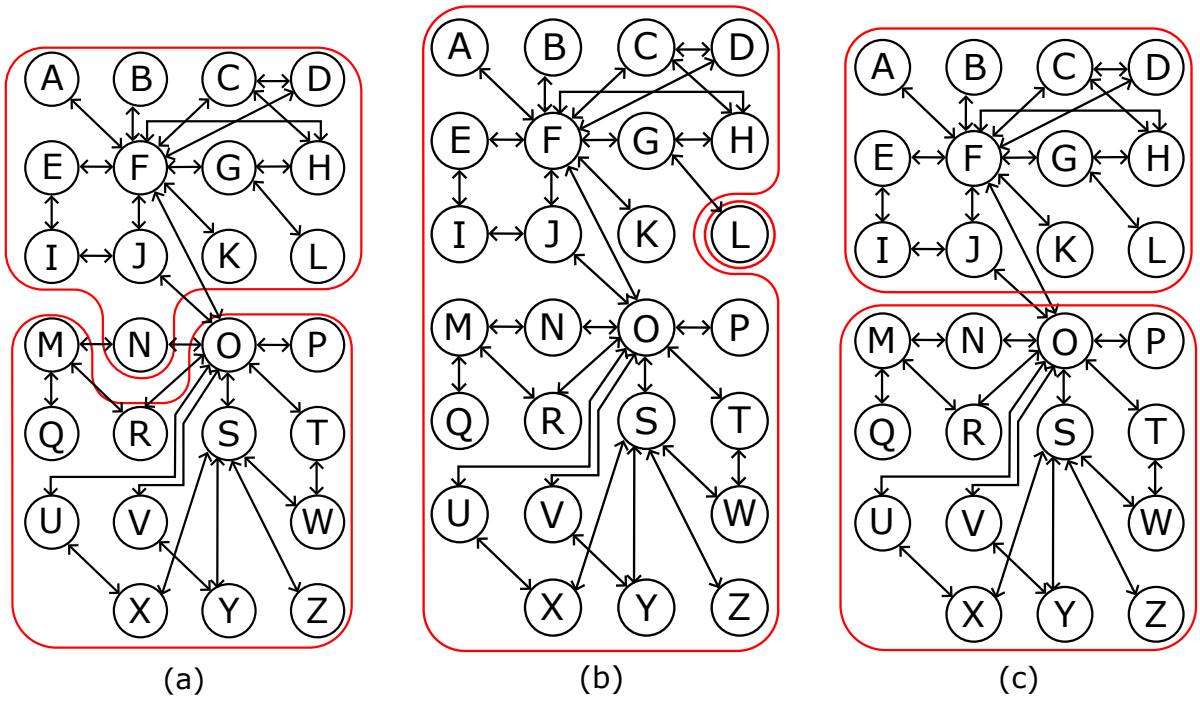

Figure 5.5.: Partitioning results of D-26-media core graph using (a) Kernighan-Lin, (b) Stoer-Wagner minimum cut, and (c) My method.

5.3. Discussion: different methods for node pairing

All the insertion loss assignments of the core graphs clustered by my method are shown in Figure A.6, Figure A.7, Figure A.8, Figure A.9 and Figure A.10 in the appendix. To compare the performance of two node pairing methods for clustered core graphs with my method, N_{sample} of the random shuffling method is set to 1000. I compare and present the maximum insertion loss, wavelength usage, and computation time in Table 5.3. The results show that the wavelength usage of the MWD core graph with the random shuffling method increases compared with the exhausted searching method because N_{sample} is set to 1000. One cluster of the MWD core graph has a dimension of 7. 7 factorial is 5040, which is larger than 1000; the sample size of the random shuffling method is insufficient to find the optimal solution. The clustered D-26-media core graph using the exhausted searching method does not have results because it has a 12-core cluster and a 14-core cluster; the computational load on the processor becomes excessive, and the computation time is longer than 3 hours. The exhausted searching method always has a shorter computation time and optimal results for the core graphs with relatively small-scale clusters. For core graphs with large-scale clusters, the random shuffling method results in shorter computation times but at the cost of losing accuracy.

Due to the factorial growth in computational complexity of the exhausted searching method with the dimension of the core graph, it becomes impractical to find the minimal maximum insertion loss of the network when the core graph scale is large. Using the heuristic method becomes relatively advantageous regarding time efficiency in this condition. Since the random shuffling method randomly selects samples from all pairing scenarios, the setting of N_{sample} largely determines its computation results and running time. Therefore, setting an acceptable N_{sample} size for large-scale core graphs can achieve a local minimum of the maximum insertion loss. For example, for a 26-core graph, the D-26-media core graph, I computed the maximum insertion loss, the wavelength usage, and the computation time for different orders of N_{sample}. According to the results in Table 5.4, when N_{sample} is set within an acceptable range for computation time, both the maximum insertion loss and the number of wavelengths used can be improved and calculated in a short time.

	Exhausted Searching Method			Random Shuffling Method		
	IL_{max}	N_{WL}	$T(s)$	IL_{max}	N_{WL}	$T(s)$
PIP	0.6	3	0.003	0.6	3	0.057
MPEG4	1.1	8	0.033	1.1	8	0.043
VOPD	0.6	4	0.005	0.6	4	0.034
MWD	0.65	3	0.015	0.65	4	0.012
D-26-media	-	-	-	1.2	12	0.043

Table 5.3.: Comparison of exhausted searching method and random shuffling method with different clustered core graphs.

N_{sample}	10^3	10^4	10^5	10^6	10^7
Time(s)	0.0413	0.356	2.932	28.022	298.7
IL_{max} (dB)	1.2	1.1	1.1	1.1	1.1
$N_{Wavelength}$	12	11	9	9	9

Table 5.4.: Average running time, insertion loss wavelength and usage of random shuffling method with a 26-core graph(D-26-media core graph).

6. Conclusion

This work primarily proposed a method based on a clustering method for partitioning the communication of WRONoCs and two methods for node pairing after partitioning and compared two partitioning algorithms, Kernighan-Lin algorithm and Stoer-Wagner minimum cut algorithm, with the method proposed in this work. Furthermore, when pairing the cores on WRONoCs with topologies' ports, employing node-pairing methods can also significantly reduce the maximum insertion loss of the entire network.

Experimental comparisons showed that compared to supporting the entire WRONoCs with a single topology, separating the core graph of WRONoCs with the method proposed in this work and supporting the clusters with smaller-scale topologies can effectively reduce the network's maximum insertion loss and wavelength usage. Using the power-aware and scalable method can improve power efficiency and significantly enhance the performance of large-scale WRONoCs.

A. Appendix

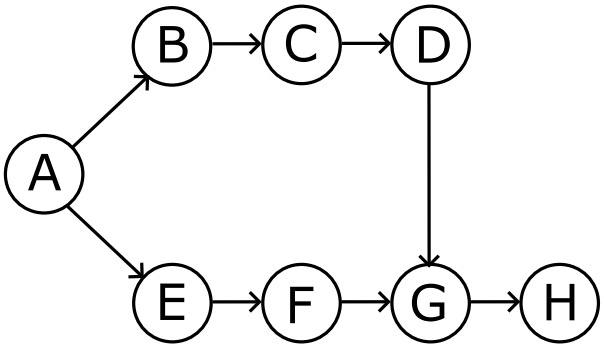

Figure A.1.: PIP core graph.

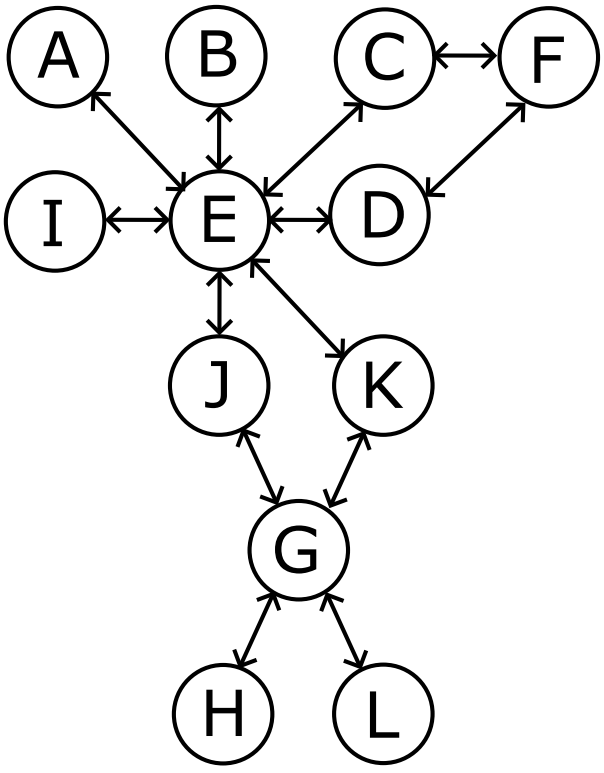

Figure A.2.: MPEG4 core graph.

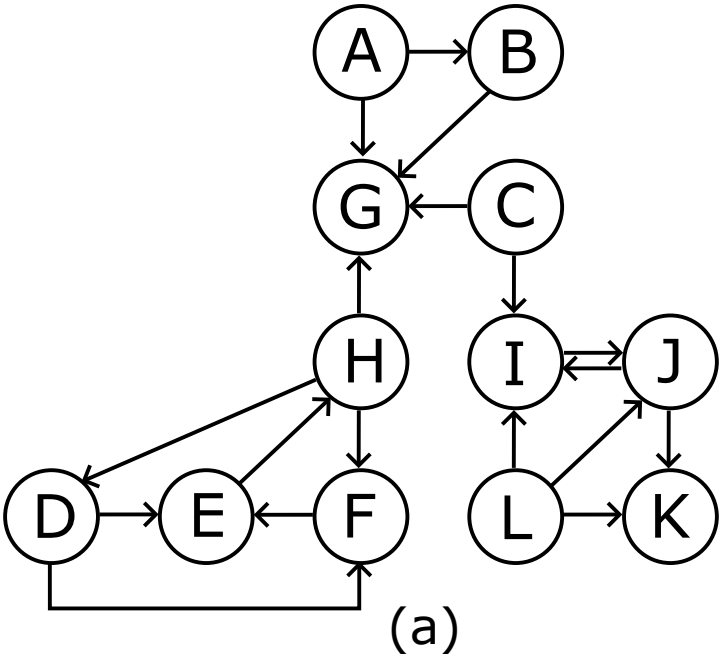

Figure A.3.: VOPD core graph.

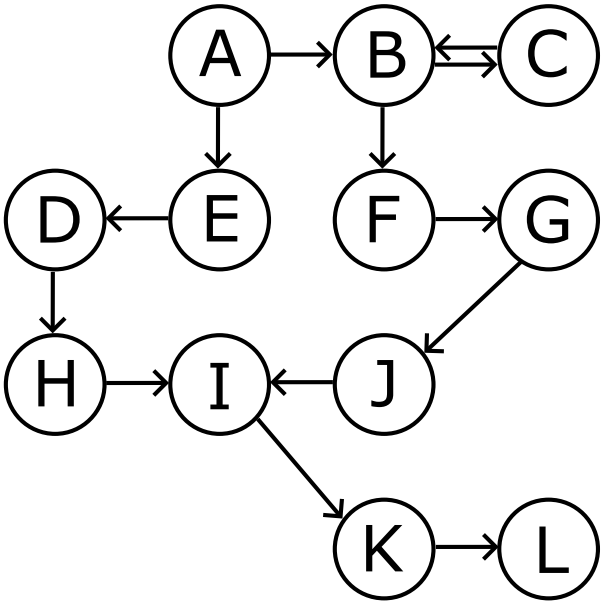

Figure A.4.: MWD core graph.

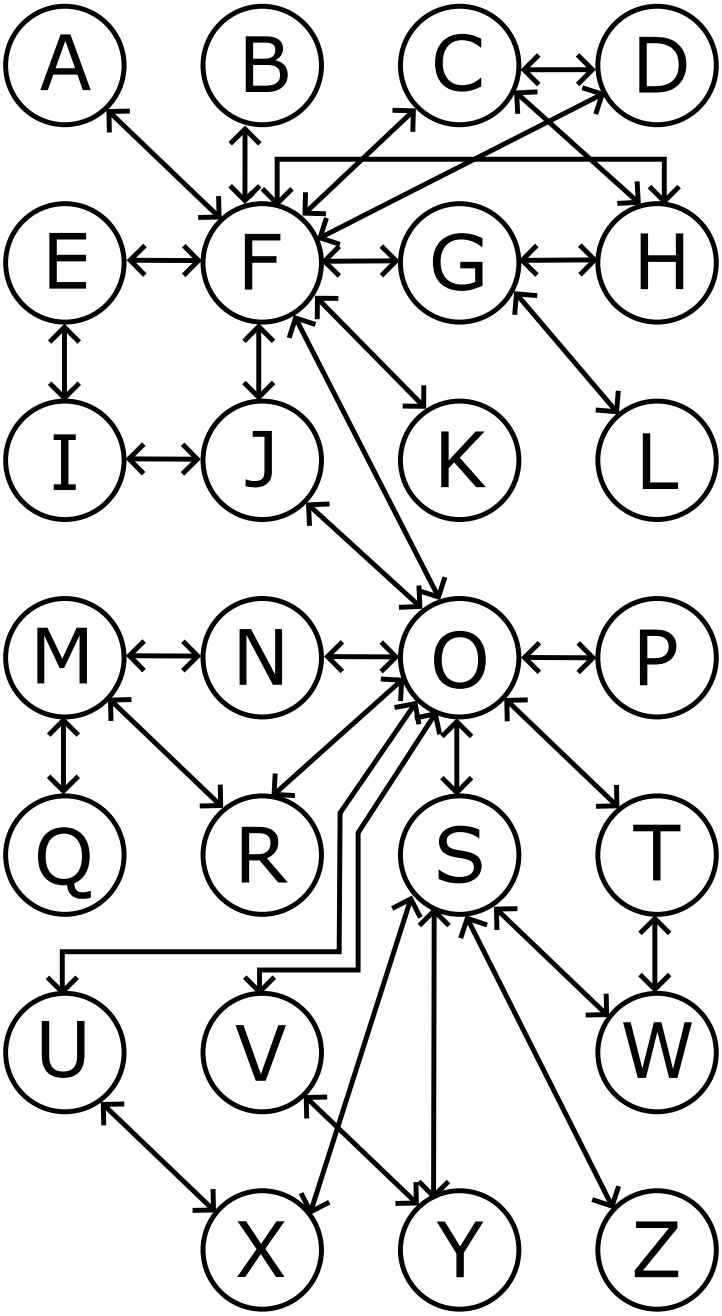

Figure A.5.: D-26-media core graph.

(dB)	O_0	O_1	O_2	O_3	O_4	O_5	O_6	O_7
I_0	-	0.6	0.7	0.8	0.9	0.8	0.7	0.3
I_1	0.5	-	0.8	0.9	0.8	0.7	0.3	0.8
I_2	0.6	0.7	-	1	0.7	0.3	0.8	0.7
I_3	0.7	0.8	0.9	-	0.3	0.8	0.7	0.6
I_4	1	0.9	0.8	0.3	-	0.5	0.6	0.7
I_5	0.9	0.8	0.3	0.7	0.6	-	0.7	0.8
I_6	0.8	0.3	0.7	0.6	0.7	0.8	-	0.9
I_7	0.3	0.7	0.6	0.5	0.8	0.9	1	-

Table A.1.: 8×8 GWOR insertion loss.

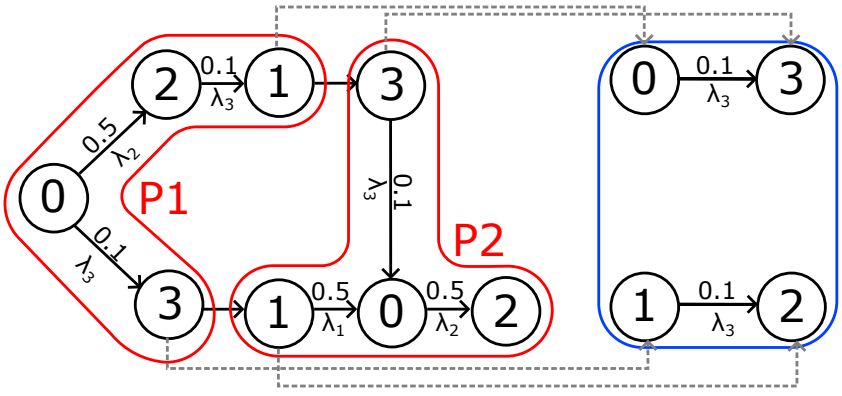

Figure A.6.: Insertion loss assignment of PIP core graph using node-pairing method.

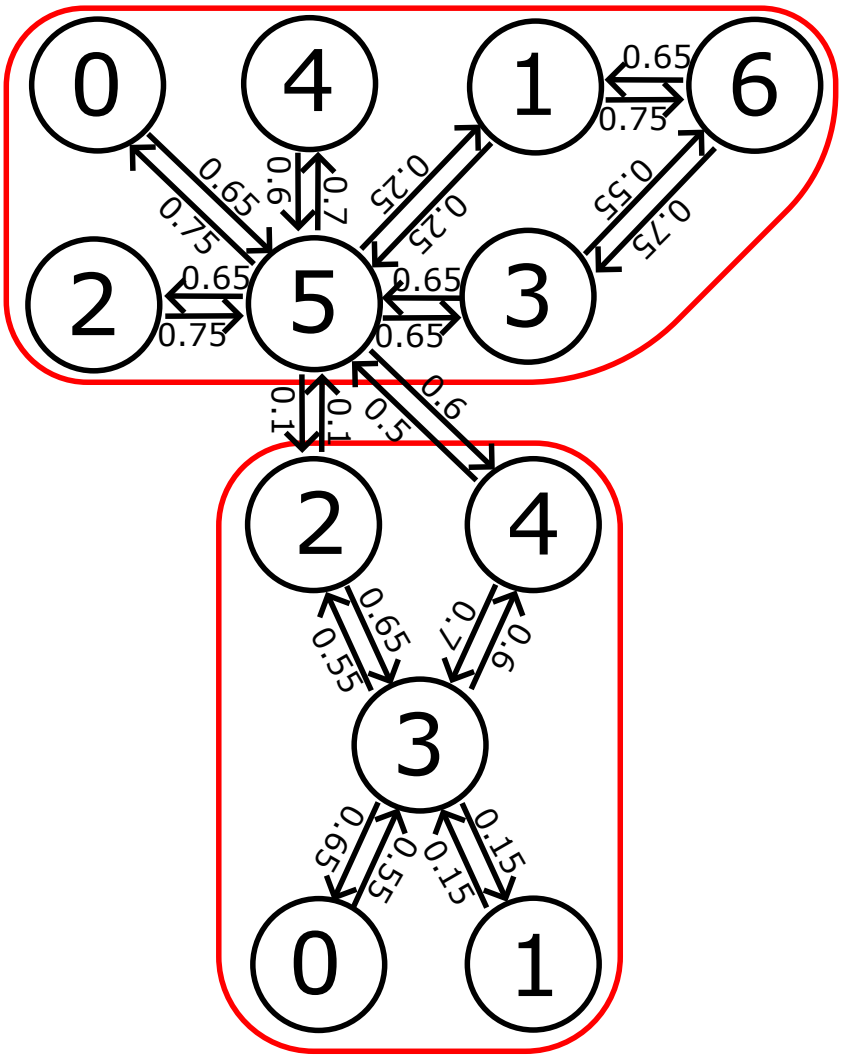

Figure A.7.: Insertion loss assignment of MPEG4 core graph using node-pairing method.

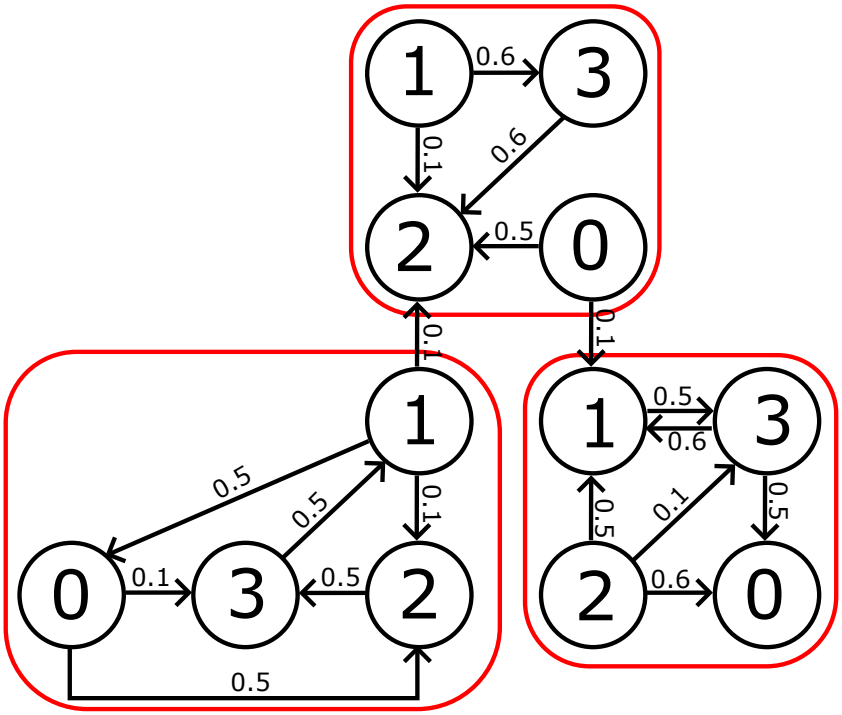

Figure A.8.: Insertion loss assignment of VOPD core graph using node-pairing method.

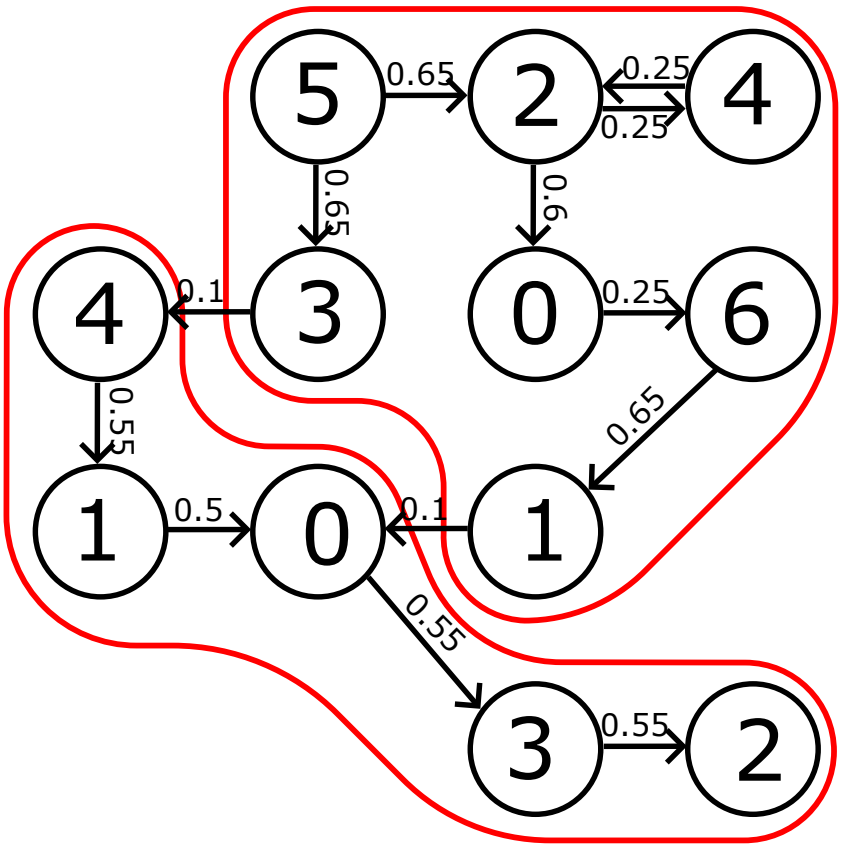

Figure A.9.: Insertion loss assignment of MWD core graph using node-pairing method.

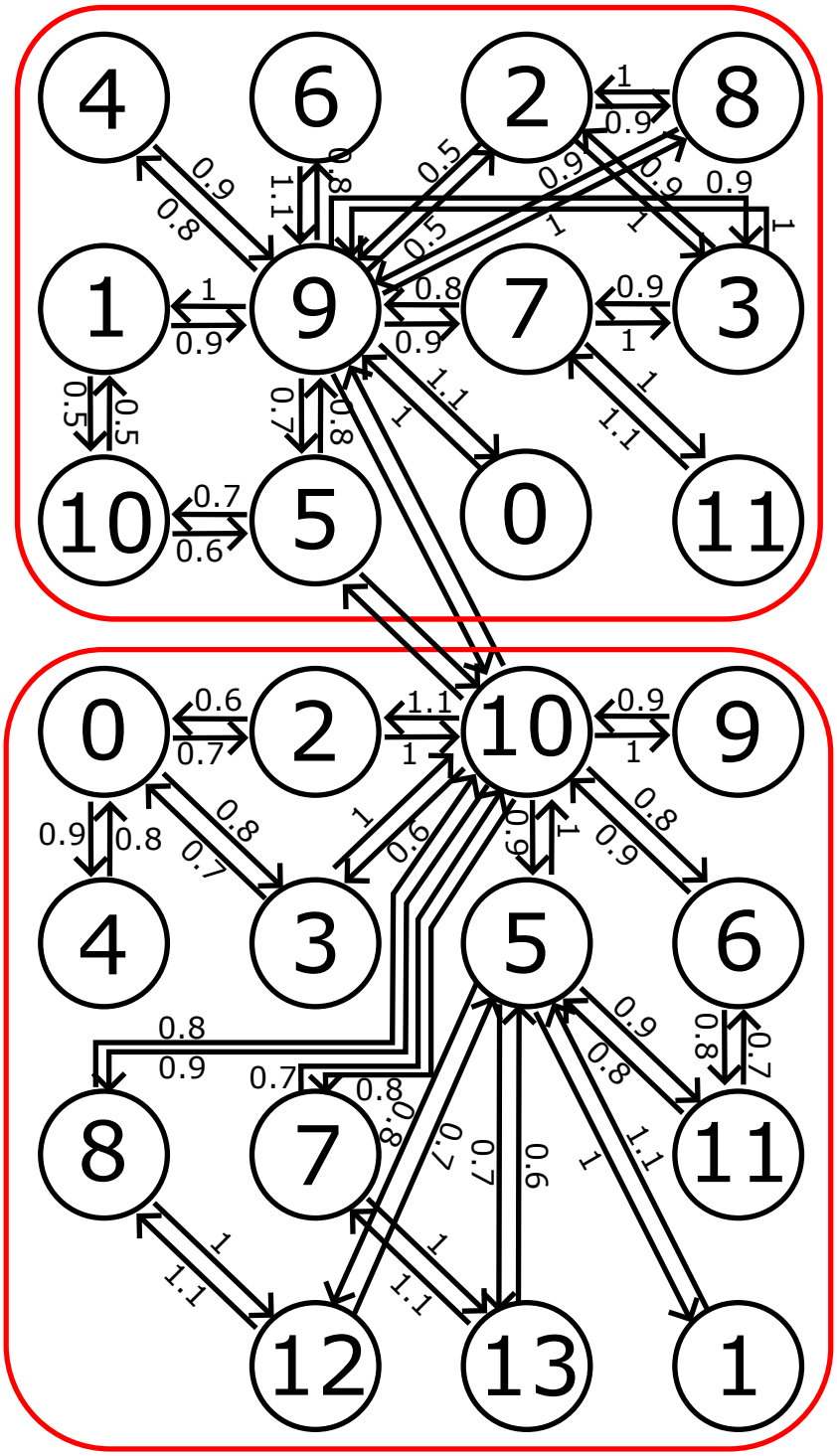

Figure A.10.: D-26-media clustered core graph using node-pairing method.

Bibliography

B. W. Kernighan, et al. (1970): An efficient heuristic procedure for partitioning graphs, The Bell System Technical Journal **49**: 291 – 307.

C. Manolatou, et al. (2002): Passive Components for Dense Optical Integration, Kluwer Academic Publishers.

C. Seiculescu, et al. (2009): SunFloor 3D: A Tool for Networks on Chip Topology Synthesis for 3-D Systems on Chips, 2009 Design, Automation & Test in Europe Conference & Exhibition .

D. Bertozzi, et al. (2005): NoC synthesis flow for customized domain specific multiprocessor systems-on-chip, IEEE Transactions on Parallel and Distributed Systems **16**: 113 – 129.

F. Wagner, et al. (1997): A simple min-cut algorithm, Journal of the ACM (JACM) **44**: 585 – 591.

L. Duong, et al. (2014): A Case Study of Signal-to-Noise Ratio in Ring-Based Optical Networks-on-Chip, IEEE Design & Test **31**: 55 – 65.

M. Briere, et al. (2007): System level assessment of an optical noc in an mpsoc platform., 2007 Design, Automation & Test in Europe Conference & Exhibition .

M. Nikdast, et al. (2015): Crosstalk Noise in WDM-Based Optical Networks-on-Chip: A Formal Study and Comparison, IEEE Transactions on Very Large Scale Integration (VLSI) Systems **23**: 2552–2565.

M. Ortin, et al. (2015): Partitioning Strategies of Wavelength-Routed Optical Networks-on-Chip for Laser Power Minimization, 2015 Workshop on Exploiting Silicon Photonics for Energy-Efficient High Performance Computing .

M. Ortín-Obón, et al. (2017): Contrasting Laser Power Requirements of Wavelength-Routed Optical NoC Topologies Subject to the Floorplanning, Placement, and Routing Constraints of a 3-D-Stacked System, IEEE Transactions on Very Large Scale Integration (VLSI) Systems **25**: 2081 – 2094.

P. Grani, et al. (2017): Design and Evaluation of AWGR-Based Photonic NoC Architectures for 2.5D Integrated High Performance Computing Systems, 2017 IEEE International Symposium on High Performance Computer Architecture (HPCA) .

T. Tseng, et al. (2019): Wavelength-Routed Optical NoCs: Design and EDA — State of the Art and Future Directions: Invited Paper, 2019 IEEE/ACM International Conference on Computer-Aided Design (ICCAD) .

X. Tan, et al. (2011): On a Scalable, Non-Blocking Optical Router for Photonic Networks-on-Chip Designs, Symp. Photonics and Optoelectronics (SOPO) .

Z. Zheng, et al. (2021a): Light: A Scalable and Efficient Wavelength-Routed Optical Networks-On-Chip Topology, 26th Asia and South Pacific Design Automation Conference (ASP-DAC) .

Z. Zheng, et al. (2021b): ToPro: A Topology Projector and Waveguide Router for Wavelength-Routed Optical Networks-on-Chip, 2021 IEEE/ACM International Conference On Computer Aided Design (ICCAD) .